

Accelerating the screening of amorphous polymer electrolytes by learning to reduce random and systematic errors in molecular dynamics simulations

Tian Xie,^{1,2} Arthur France-Lanord,^{1,2} Yanming Wang,^{1,2} Jeffrey Lopez,² Michael Austin Stolberg,^{1,3} Megan Hill,³ Graham Michael Leverick,⁴ Rafael Gomez-Bombarelli,¹ Jeremiah A. Johnson,³ Yang Shao-Horn,^{1,4} and Jeffrey C. Grossman^{1,2}

¹*Department of Materials Science and Engineering,
Massachusetts Institute of Technology,
Cambridge, Massachusetts 02139, United States*

²*Research Laboratory of Electronics,
Massachusetts Institute of Technology,
Cambridge, Massachusetts 02139, United States*

³*Department of Chemistry, Massachusetts Institute of Technology,
Cambridge, Massachusetts 02139, United States*

⁴*Department of Mechanical Engineering,
Massachusetts Institute of Technology,
Cambridge, Massachusetts 02139, United States*

Abstract

Machine learning has been widely adopted to accelerate the screening of materials. Most existing studies implicitly assume that the training data are generated through a deterministic, unbiased process, but this assumption might not hold for the simulation of some complex materials. In this work, we aim to screen amorphous polymer electrolytes which are promising candidates for the next generation lithium-ion battery technology but extremely expensive to simulate due to their structural complexity. We demonstrate that a multi-task graph neural network can learn from a large amount of noisy, biased data and a small number of unbiased data and reduce both random and systematic errors in predicting the transport properties of polymer electrolytes. This observation allows us to achieve accurate predictions on the properties of complex materials by learning to reduce errors in the training data, instead of running repetitive, expensive simulations which is conventionally used to reduce simulation errors. With this approach, we screen a space of 6247 polymer electrolytes, orders of magnitude larger than previous computational studies. We also find a good extrapolation performance to the top polymers from a larger space of 53362 polymers and 31 experimentally-realized polymers. The strategy employed in this work may be applicable to a broad class of material discovery problems that involve the simulation of complex, amorphous materials.

INTRODUCTION

Polymer electrolytes are promising candidates for next generation lithium-ion battery technology due to their low cost, safety, and manufacturing compatibility. The major challenge with the current polymer electrolytes is their low ionic conductivity, which limits the usage in real world applications. [1–3] This limitation has motivated tremendous research efforts to explore new classes of polymers via both experiments [4–7] and atomic scale simulations [8–10]. However, the simulation of ionic conductivity is extremely expensive due to the amorphous nature¹ of polymer electrolytes and the diversity of timescales involved in their dynamics, drastically limiting the ability to employ high throughput computational screening approaches. For instance, recent studies [8–10] exploring polymer electrolytes with classical molecular dynamics (MD) only simulated around ten polymers. In contrast, a study that applies machine learning methods to literature data is able to explore a larger chemical space [7], but it is limited by the diversity of polymers that have been studied in the past. The exploration beyond known chemical spaces would require a significant acceleration of the computational screening of polymer electrolytes.

There are two major reasons for the large computational cost for simulating the ionic conductivity of polymer electrolytes with MD. First, the amorphous structure of polymer electrolytes can only be sampled from a random distribution using, e.g., Monte Carlo algorithms, and yet this initial structure has a significant impact on the simulated ionic conductivity due to the lack of ergodicity in the MD simulation [10, 11]. Multiple simulations starting from independent configurations are therefore required in order to properly sample the phase space and reduce statistical noise. Second, the slow relaxation of polymers requires long MD simulation time to achieve convergence for ionic conductivity (on the orders of 10’s to 100’s of ns), so each MD simulation is also computationally expensive [8, 10].

Machine learning (ML) techniques have been widely used to accelerate the screening of ordered materials [12, 13], but most previous studies implicitly [14–17] assume that the properties used to train the ML models are generated through a deterministic, unbiased process. However, the MD simulation of complex materials like amorphous polymers is intrinsically stochastic, and obtaining data with low statistical uncertainties by running

¹ Strictly speaking, polymers have different degrees of crystallinity and are not completely amorphous. In this work, we use the term amorphous materials to represent a range of solids from fully amorphous to semi-crystalline. They cannot be represented by a simple periodic structure and thus are generally difficult to simulate.

repetitive simulations is impractical at a large scale due to the large computational cost. An alternative approach is to reduce the accuracy requirements for individual MD simulations and learn to reduce the random and systematic errors with large quantities of less expensive, yet imperfect data. It has previously been demonstrated that ML models can learn from noisy data and recover the true labels for images [18] and graphs [19]. Past works have also shown that systematic differences between datasets can be learned employing transfer learning techniques. [20–23] Inspired by these results, we hope to significantly reduce the computational cost for simulating the transport behavior of polymers by adopting a noisy, biased simulation scheme with short, unconverged MD simulations.

In this work, we aim to accelerate the high throughput computational screening of polymer electrolytes by learning from a large amount of biased, noisy data and a small number of unbiased data from molecular dynamics simulations. Despite the large random errors caused by the dependence on initial structure, we only perform one MD simulation for each polymer, and learn a shared model across polymers to reduce the random error and recover true properties that one would obtain from repetitive simulations. To reduce the long MD simulation time, we perform large quantities of short, unconverged MD simulations and a small number of long, converged simulations. We then employ multi-task learning to learn a correction from the short simulation properties to long simulation properties. We find that our model achieves a prediction error with respect to the true properties smaller than the random error from a single MD simulation, and it also corrects the systematic errors from unconverged simulations better than a linear correction. Combining the reduction of both random and systematic errors, we successfully screen a space of 6247 polymers and discover the best polymer electrolytes from the space, which corresponds to a 22.8-fold acceleration compared with simulating each polymer directly with one long simulation. Finally, we extrapolate our model into a larger space of 53362 polymers with more complex monomer structures, and we validate our predictions with 31 experimentally studied polymers.

RESULTS

Polymer space and sources of errors. The polymer space we aim to explore is defined in Fig. 1(a), which considers both the synthesizability of polymers and their potential as electrolytes. In general, it is difficult to determine the synthesizability, especially the

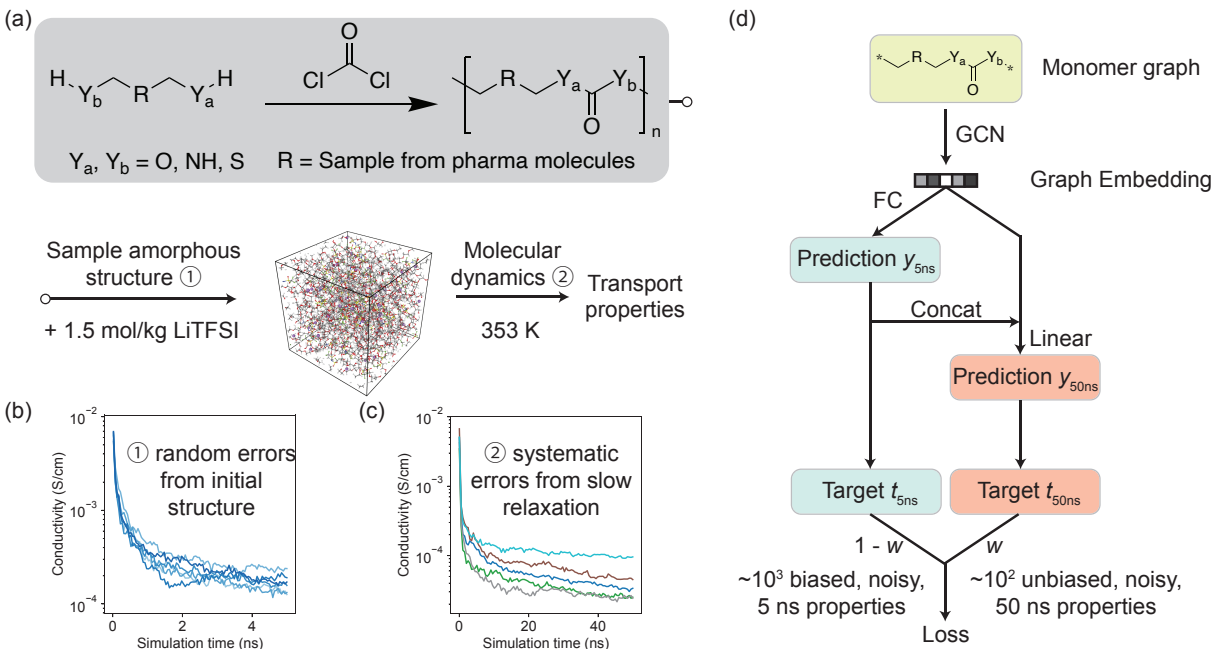


FIG. 1. Illustration of the polymer space and the learning framework. (a) The polymer space and molecular dynamics simulation workflow. (b) Ionic conductivity as a function as simulation time from 6 independent 5 ns MD runs for the same polymer, showing the random errors caused by the amorphous structure initialization. (c) Ionic conductivity as a function as simulation time for 5 different polymers, showing the long simulation time needed for convergence. (Polymer structures for (b, c) are provided in the supplementary information.) (d) Multi-task learning framework to reduce the random and systematic errors from MD simulations.

polymerizability, of an unknown polymer. Here we focus on a well established condensation polymerization route using carbonyl dichloride and comonomers containing any combination of two primary hydroxyl, amino, or thiol groups to form poly-carbonates, ureas, dithiocarbonates, urethanes, thiourethanes, and thiocarbonates. This scheme does not guarantee polymerizability, but provides a likely route for lab synthesis. The carbonyl structure ensures a minimum capability to solvate Li-ions as an electrolyte, and it also allows for the maximum diversity of polymer backbones. The monomers are sampled from a large pharmaceutical database [24] to ensure its structures are realistic. After obtaining the molecular structure of the polymer, we sample its 3D amorphous structure with a Monte Carlo algorithm, insert 1.5 mol lithium bis(trifluoromethanesulfonyl)imide (LiTFSI) salt per kilogram of polymer, perform a 5 ns MD equilibration, and finally run the MD simulation to compute

its transport properties like conductivity.

There are mainly two types of errors in this workflow. In the scope of this work, we call random errors the ones that can be eliminated by running repetitive simulations on the same polymer, and systematic errors those that cannot be eliminated. The major source of random error is the sampling of initial amorphous structure of the polymer. In Fig. 1(b), we show the conductivities computed from 6 different random initializations for the same polymer, which has a large standard deviation of $0.094 \log_{10}(\text{S/cm})$ in the log scale at 5 ns. This error comes from the lack of ergodicity of MD simulations for polymers – the large scale amorphous structure of the polymers usually does not change significantly at the timescale that can be achieved with MD. The systematic errors mainly come from the long MD simulation time needed to obtain the converged conductivity. Fig. 1(c) shows the value of conductivity as a function of the simulation time for 5 different polymers, which slowly converges as the simulation progresses. This slow convergence introduces a systematic error of ionic conductivity with any specified simulation time with respect to the converged conductivity. On average, there is a $0.435 \log_{10}(\text{S/cm})$ difference in the log scale between a 5 ns and a 50 ns simulation for these 5 polymers. Here, we use the 50 ns simulation results as the converged values, although it is not fully converged for some polymers. Based on our comparison with respect to experimental values reported in literature [4, 6, 25–34] in Fig. S1, the 50 ns simulation has a reasonable agreement except for polymers with very low conductivity. Note that even 50 ns conductivities have large random errors similar to the 5 ns conductivities, since the random errors are mainly caused by the large scale amorphous structures that do not change significantly with long simulation time.

Multi-task model to reduce errors. These two types of errors introduce significant computational costs to achieve an accurate calculation of ionic conductivity for individual polymers, because such a calculation requires repetitive simulations on the same polymer that are also individually expensive. Here we attempt to reduce these errors by learning a shared model across the polymer space. To achieve this goal, we develop a multi-task graph neural network architecture (Fig. 1(d)) to learn to reduce both random and systematic errors from MD simulations. We first encode the monomer structure as a graph \mathcal{G} (details of the encoding discussed in the methods section) and use a graph neural network G to learn a representation for the corresponding polymer, $\mathbf{v}_{\mathcal{G}} = G(\mathcal{G})$. Here we use a CGCNN [35] as G , similar to previous works that employ graph convolutional networks (GCNs) in polymers

[36, 37].

To build a predictor that reduces random errors, we use the robustness of neural networks against random noises in the training data, previously demonstrated in images [18] and graphs [19]. We assume that there exists a true target property (e.g. conductivity) that is uniquely determined by the structure of the polymer (which would require infinite repetitive simulations to obtain), and the computed target property from MD is slightly different from the true property due to the random errors in the simulation. This assumption can be written as,

$$t = f(\mathcal{G}) + \epsilon, \quad (1)$$

where t is the target property computed from MD, f is a deterministic function mapping from monomer structure to true polymer property, and ϵ is a random variable independent of \mathcal{G} with zero mean. Note that ϵ should be a function of \mathcal{G} in principle, but similar noise is observed across polymers as shown in Fig. S2 and assuming ϵ is independent of \mathcal{G} simplifies our analysis. By regressing over t , it is possible to learn $f(\mathcal{G})$ even when the noise is large [18] if enough training data is available. To generate a large amount of training data, since 50 ns simulations are too expensive practically, we use less accurate 5 ns simulations to generate training data and use a network g_1 to predict $t_{5\text{ ns}}$ with the graph representation,

$$y_{5\text{ ns}} = g_1(\mathbf{v}_{\mathcal{G}}). \quad (2)$$

With enough training data generated using the affordable 5 ns simulations, we can learn an approximation to the true property function $f_{5\text{ ns}}$ despite the random errors. However, there is a systematic error between $f_{5\text{ ns}}$ and $f_{50\text{ ns}}$ due to the slow relaxation of polymers. To correct this error, we perform a small amount of 50 ns simulation to generate data for the converged conductivities. This correction can then be learned with a linear layer g_2 using both predictions from 5 ns simulations and the graph representations,

$$y_{50\text{ ns}} = g_2(\mathbf{v}_{\mathcal{G}} \parallel y_{5\text{ ns}}), \quad (3)$$

where \parallel denotes concatenation.

Finally, the two datasets, a larger 5 ns dataset and a smaller 50 ns dataset, can be trained jointly using a combined loss function,

$$\text{Loss} = (1 - w) \cdot \frac{1}{N_{5\text{ ns}}} \sum_{\mathcal{G}_{5\text{ ns}}} (y_{5\text{ ns}} - t_{5\text{ ns}})^2 + w \cdot \frac{1}{N_{50\text{ ns}}} \sum_{\mathcal{G}_{50\text{ ns}}} (y_{50\text{ ns}} - t_{50\text{ ns}})^2, \quad (4)$$

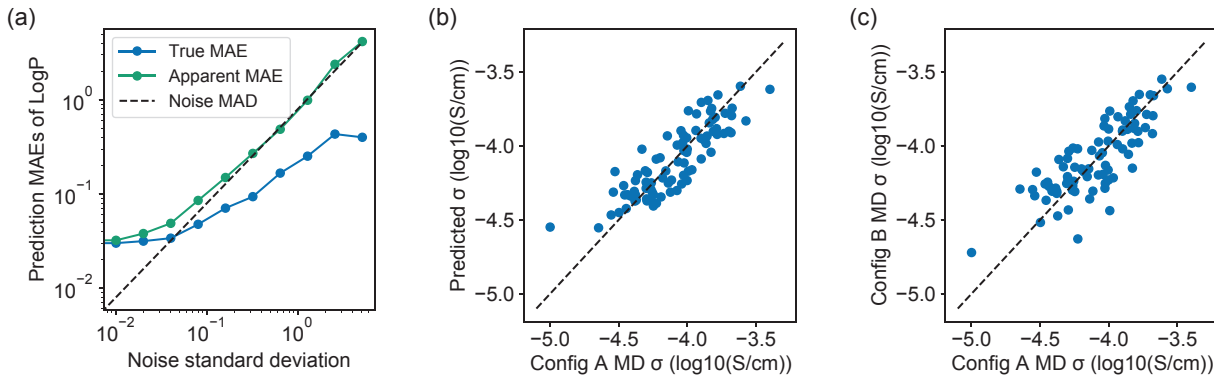


FIG. 2. Performance on reducing random errors. (a) Mean absolute errors (MAEs) on a toy dataset to predict LogP with increasing noises in training data. Blue line denotes MAEs with respect to true LogP values, green line denotes MAEs with respect to noisy LogP values, and dashed line denotes the mean absolute deviation (MAD) of the Gaussian noise. (b) Scatter plot comparing the predicted conductivity and computed conductivity from one initialization (config A) in the test dataset. (c) Scatter plot comparing conductivities from two independent initializations (config A and config B) for the same polymers in the test dataset.

where w is a weight between 0 and 1.

Using an iterative scheme, we sampled the entire polymer space in Fig. 1(a) with both 5 ns and 50 ns simulations. The 5 ns dataset includes 876 polymers and the 50 ns dataset includes 117 polymers. Note that we only simulate each polymer once so there is no duplicate in both datasets. We leave 10% of the polymers in both datasets as test data, and use 10-fold cross validation on the rest of the data to train our models. Due to the small size of the 50 ns dataset, we use stratified split while dividing the data to ensure that the training, validation, test data contain polymers with the full range of conductivities [38]. In the next sections, we first demonstrate the performance of our model based on these two datasets and then discuss the iterative screening of the polymer space.

Performance on reducing random errors. To demonstrate that our model can recover the true properties from noisy data, we first study a toy dataset for which we have access to the true property $f(\mathcal{G})$ in Eq. 1. We use the same dataset from 5 ns simulations and compute the partition coefficient, LogP, of each polymer using Crippen’s approach [39, 40], which uses an empirical equation whose output is fully determined by the molecular structure. Then, we add different levels of Gaussian random noise into the LogP values to

imitate the random errors in simulated conductivities. Here, we only use the g_1 branch of our model, i.e. $w = 0$, to predict LogP values from the synthesized noisy data. Fig. 2(a) shows the true mean absolute errors (MAEs) with respect to the original LogP values and apparent MAEs with respect to the noisy LogP values as a function of the standard deviation of the Gaussian noise, on a test dataset including 86 polymers. We observe that the true MAEs become smaller than the mean absolute deviation (MAD) of the Gaussian noise when the noise standard deviation is larger than 0.08. This result shows that our model predicts LogP more accurately than performing a noisy simulation of LogP due to the existence of large random error in the simulation.

We cannot use the same approach to evaluate the model performance on predicting simulated 5 ns conductivities because we do not have access to the true conductivities. Instead, we can only compute the apparent MAE on 86 test data, which is $0.117 \log_{10}(\text{S/cm})$ in Fig. 2(b). To compare our prediction performance with performing a 5 ns MD simulation, we run another independent MD simulation for each test polymer and compare the MAE between the two simulations. The MAE in Fig. 2(c) is $0.132 \log_{10}(\text{S/cm})$, slightly larger than the apparent prediction MAE. This result indicates that our prediction of the noisy conductivity also outperforms an independent MD simulation due to its large random noise, similar to the LogP prediction. To estimate the true prediction performance with respect to the inaccessible true conductivity, we need to assume that the random errors for 5 ns MD conductivity follow a Gaussian distribution, which is approximately correct (Fig. S2). We could then estimate the true root mean squared error (RMSE) to be $0.085 \log_{10}(\text{S/cm})$, smaller than the standard deviation of the Gaussian noise $0.117 \log_{10}(\text{S/cm})$ (detailed calculations can be found in supplementary note 1). This finding shows that the error in our prediction of 5 ns simulated conductivity is smaller than a 5 ns MD simulation due to its random errors.

Performance on correcting systematic errors. In addition to reducing random errors, our model is also able to learn the systematic difference between 5 ns and 50 ns MD simulated properties with the multi-task scheme. After co-training our model with both 5 ns and 50 ns datasets, we present the predictions on 11 test data from 50 ns MD in Fig. 3(a). Compared with the original 5 ns conductivities, our model corrects the systematic error and achieves a MAE of $0.076 \log_{10}(\text{S/cm})$ by averaging the predictions from 10-fold cross validations. It is clear that the model corrects the systematic error by learning a customized correction to each polymer, which is better than an overall linear correction which gives a

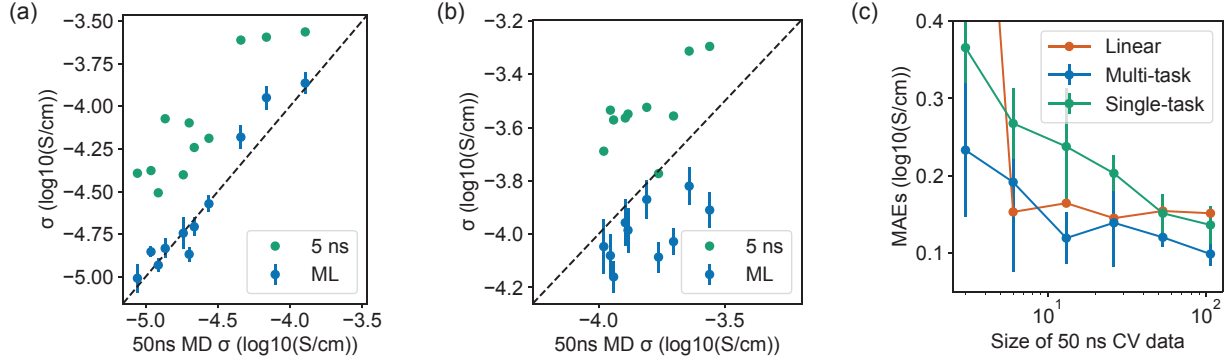


FIG. 3. Performance on correcting systematic errors. (a-b) Scatter plots showing the interpolation (a) and extrapolation (b) performance of the model on test data. Blue and green dots present the results of 5 ns MD simulations and ML predictions compared with 50 ns MD conductivities, respectively. The error bars represent the standard deviations of predictions from 10-fold cross validation. (c) Change of interpolation performance with different number of CV data. The red, blue, green lines denote the MAEs of linear correction, multi-task model, and single-task model predicting 50 ns conductivity. The error bars represent the standard deviations of MAEs from 10-fold cross validation.

MAE of $0.152 \log_{10}(\text{S/cm})$. Note that this MAE does not include random errors, because our 5 ns and 50 ns conductivities are computed from the same random initial structures. The results in Fig. 3(a) represent the interpolation performance of our model since we randomly split our data. To further study the extrapolation performance, we perform the same co-training but reserve the top 10 polymers with highest conductivity as test data. In Fig. 3(b), we find that by training with low-conductivity polymers, the model underestimates the 50 ns conductivity and achieves a MAE of $0.182 \log_{10}(\text{S/cm})$. This underestimation is due to the larger systematic error between 50 ns and 5 ns conductivities in training data, caused by slow relaxations in low-conductivity polymers. Nevertheless, the model still performs better than a linear correction that only has access to the training data, which has a MAE of $0.275 \log_{10}(\text{S/cm})$.

In Table I, we study how the systematic error correction performs for other transport properties, including lithium ion diffusivity (D_{Li}), TFSI diffusivity (D_{TFSI}), and polymer diffusivity (D_{Poly}). Both interpolation and extrapolation performances are reported similar to the results of conductivity. To better evaluate the uncertainties caused by the small

TABLE I. Comparison of the mean absolute errors (MAEs) on predicting 50 ns MD simulated properties between different approaches. For each property, interpolation and extrapolation performance are represented by labels without and with the * symbol. Uncertainties are the standard deviations of MAEs from 10-fold cross validation (CV).

Method	σ	σ^*	D_{Li}	D_{Li}^*	D_{TFSI}	D_{TFSI}^*	D_{Poly}	D_{Poly}^*
5 ns	0.528	0.278	0.503	0.419	0.455	0.249	0.612	0.528
5 ns (linear)	0.152	0.275	0.148	0.247	0.096	0.297	0.072	0.110
ML CV	0.093 ± 0.017	0.186 ± 0.053	0.106 ± 0.016	0.209 ± 0.050	0.101 ± 0.020	0.181 ± 0.028	0.072 ± 0.019	0.114 ± 0.030
ML average	0.076	0.182	0.080	0.202	0.075	0.171	0.056	0.104

50 ns dataset, we compute the mean and standard deviation of the prediction MAEs from each fold of 10-fold cross validation in *ML CV*. This MAE is different from our previous MAEs, denoted as *ML average*, which uses the mean from cross validations to make a single prediction. Overall, *ML average* outperforms a linear correction for all properties, indicating the generality of the customized correction of systematic errors. However, there is a relatively high variance between different folds of cross validation due to the small data size, especially for the extrapolation tasks. *ML CV* performs the same or slightly worse than a linear correction for D_{TFSI} , D_{Poly} , and D_{Poly}^* . A potential explanation is that a linear correction already performs reasonably well for these properties, demonstrated by the small MAEs of linear correction, while a more complicated multi-task model is prone to overfitting the noises in a small 50 ns dataset.

In Fig. 3(c), we further study how the performance of our model would evolve with less 50 ns data, since these long MD simulations are expensive to run and cannot be easily parallelized. We find that the performance of the multi-task model decreases relatively slowly with less training data, and it still has some correction ability even with 13 CV data points, despite the large uncertainties due to the small data size. This observation shows the advantage of co-training a larger 5 ns dataset and a smaller 50 ns dataset – it is much easier to learn a systematic correction than learn the property from scratch, and the co-training allows the transfer of graph representation learning from the 5 ns dataset to the 50 ns dataset. In contrast, the performance of a single-task model directly predicting 50 ns

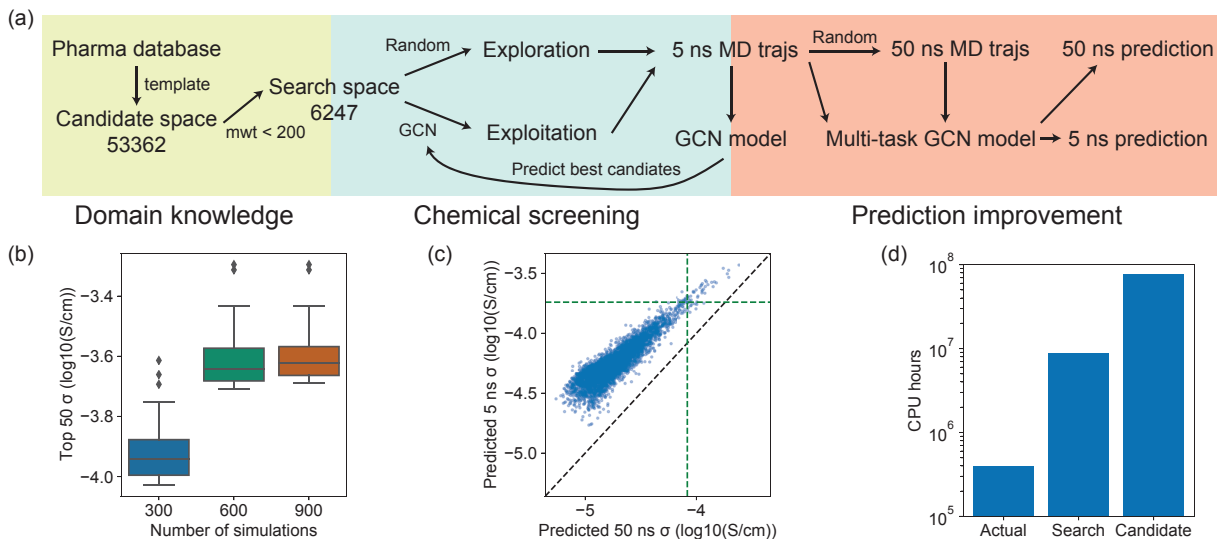


FIG. 4. Screening of polymer electrolytes. (a) Illustration of the screening workflow. (b) Distribution of the conductivities of top 50 polymers after each iteration. (c) Predictions of 50 ns and 5 ns conductivities for 6247 polymers in the search space. Green line denotes the top 50 conductivity from both predictions. (d) CPU hours that are actually used, required to screen the entire 6247 search space, and required to screen the 53362 candidate space.

conductivity degrades much faster with less training data.

Acceleration of the screening of polymers. After demonstrating the performance of the multi-task model on reducing both random and systematic errors, we employ this model to perform an extensive screening of polymer electrolytes in the polymer space defined in Fig. 1(a). The goal of the screening is to search for polymers with the highest conductivity. As shown in Fig. 4(a), we obtain 53362 polymer candidates using polymerization criteria from the ZINC chemical database [24]. To reduce the average computational cost, we limit our search space to only include polymers with monomer molecular weight less than 200, resulting in 6247 polymers.

We first use 5 ns MD simulations and a single-task GCN to explore polymers in the search space. To reduce computational cost, we only simulate each polymer once and employ GCN to reduce the random errors in the simulation. We perform 300 simulations in each iteration, 150 on randomly sampled polymers and 150 on best polymers predicted by GCN, which balances the exploration and exploitation. As shown in Fig. 4(b), the conductivities of the top 50 polymers gradually increase as more polymers are explored with the iterative approach.

But after 900 simulations, the average conductivity only increases slightly, indicating that we have achieved the best polymers in the 6247 search space based on 5 ns simulations.

Due to the systematic differences between 5 ns and 50 ns simulations, we randomly sample 120 polymers from those 900 polymers (876 successful simulations) and perform additional 50 ns MD, in which 117 are successful. These data allow us to correct the systematic errors in 5 ns simulation using the multi-task model. In Fig. 4(c), we use the multi-task model to predict the 50 ns and 5 ns conductivities of all 6247 polymers in the search space. As a result of the customized correction, the ordering of conductivity changes from 5 ns to 50 ns predictions. The Spearman’s rank correlation coefficient between these two predictions is 0.852, indicating that the ordering change is small but significant. For the top 50 polymers from 5 ns predictions, only 37 remain in the top 50 based on 50 ns predictions. This ordering change shows that the correction of systematic errors help us to identify some polymers that might be disregarded if only 5 ns simulations are performed.

To estimate the amount of acceleration we achieve, we compare the actual CPU hours used to the CPU hours that would be required if we performed one 50 ns MD simulations for each polymer. These simulations are run on NERSC Cori Haswell Compute Nodes and the CPU hours are estimated by averaging 100 simulations. In total, we use approximately 394,000 CPU hours for the MD simulations, with 33.2% for sampling and relaxing amorphous structure, 28.6% for 5 ns MD, and 38.2% for 50 ns MD. The total cost only accounts for around 4.4% and 0.51% of the computation needed to simulate all the polymers from the 6247 search space and the 53362 candidate, respectively. Note that this conservative estimation assumes that only one 50 ns MD simulation is performed for each polymer for the brute-force screening. As shown in the previous section, our model has a true prediction error smaller than the random error from a 5 ns MD simulation. Although the random error from 50 ns simulation might be smaller, our model may have a larger acceleration due to the effect of random error reduction.

Validation of the best candidates from the screening. We employ the learned multi-task model to screen all 6247 polymers in the search space and 53362 polymers in the candidate space. In Fig. 5(a), we use 50 ns MD to simulate 10 polymers out of the top 20 in the search space and 14 polymers out of the top 50 in the candidate space. These polymers are randomly selected from the top polymers using Butina clustering [40, 41] to reduce their structural similarity, and only polymers which have not been seen in the 50 ns

dataset are selected. We observe a MAE of $0.120 \log_{10}(\text{S/cm})$ and $0.093 \log_{10}(\text{S/cm})$ for the predictions in search space and candidate space, respectively, which are between the interpolation and extrapolation errors in Fig. 3 and Table I. It shows that the extrapolation to the candidate space is easier than our hypothetical extrapolation test in Fig. 3(b), yet a similar underestimation of conductivity is observed in the extrapolation. The larger errors for the top polymers in the search space might be explained by a combination of extrapolation errors and random errors in 50 ns MD simulations. We summarize the structure of the top polymers in Table S1 and S2, and most of them have PEO-like substructures which might explain their relative high conductivity.

In Fig. 5(b), we further validate the prediction of the model by gathering experimental conductivities for 31 different polymers from literature which are measured at the same salt concentration and temperature as our simulations [4, 6, 25–34], and the results are also summarized in Table S3. Note that some polymers, like polyethylene oxide (PEO), do not follow the same structure pattern as our polymers. Nevertheless, the model still gives reasonable prediction on these out-of-distribution polymers because there are many PEO-like polymers in the training data. The largest errors come from the polymers with experimental conductivity less than 10^{-5} S/cm. In general it is difficult to simulate the conductivity of polymers with such low conductivity due to the long MD simulation time needed for convergence. In Fig. S3, we observe a much smaller prediction error with respect to 50 ns MD simulated conductivities for these polymers, indicating that the error with respect to the experiments are likely caused by the limited simulation time in MD. Other than the difficulty of simulating low-conductivity polymers, possible causes of the error also include the inaccuracy of the force fields, the finite length of the polymer chain, the finite size of the simulation box, etc. For the top polymers like PEO, we observe an underestimation of conductivity because the model cannot extrapolate to these polymers that are significantly different from the training data.

DISCUSSION

We have performed a large scale computational screening of polymer electrolytes by learning to reduce random and systematic errors from molecular dynamics simulation with a multi-task learning framework. Our screening shows that PEO-like structure is the opti-

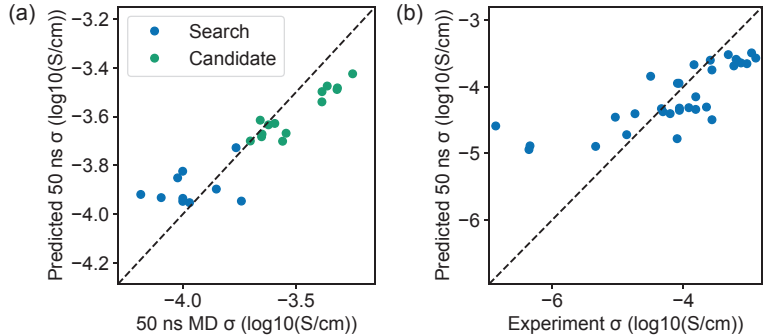


FIG. 5. Validation of the predicted polymers. (a) Validation of the best candidates from the search space (blue) and the candidate space (green). (b) Validation of the model prediction with out-of-distribution literature data.

num structure for a broad class of carbonyl-based polymers. This finding is not surprising given that PEO has been one of the best polymer electrolyte since its discovery in 1973 [42]. However, with the large space of polymers screened in this work, our results reconfirm the advantage of PEO-like structures with respect to a broad range of chemical structures. Several potential directions remain open for discovering polymer electrolytes better than PEO. The first is to search for polymer electrolytes that achieve optimum conductivity at very high salt concentrations. Conductivity generally increases with increased salt concentration, but ion clustering and decreased diffusivity will reduce conductivity at high concentrations. [1] Our screening keeps a constant concentration of 1.5 mol/kg LiTFSI for different polymers, but some polycarbonate electrolytes show advantage at an extremely high salt concentrations [43, 44]. The second is to explore polymer chemistry beyond this study. Due to the limitations of the Monte Carlo procedure used to generate initial configurations, our simulations do not include polymers with aromatic rings. Recent studies propose the potential of polymers with high fragility and aromatic rings as polymer electrolytes due to the decoupling of ionic conductivity from structural relaxation [45]. Backbones containing different lewis acidic heteroatoms or non-carbonyl based motifs could also lead to better polymer electrolytes. [9]

The large scale screening is possible because we significantly reduce the computational cost of individual simulations by learning from imperfect data with the multi-task learning framework. The ability of neural networks to learn from noisy data is extensively studied

in machine learning [18, 46, 47] and has recently been applied to reduce the signal-to-noise ratio of band-excitation piezoresponse force microscopy [48] in materials science. Despite the wide use of graph neural networks in material discovery [16, 49, 50], the random errors in training data are less studied, possibly because previous studies focus on simpler materials of which the random errors are much smaller. We show that random errors can be effectively reduced by learning a graph neural network across different chemistry even when the random error for each simulation is significant. It provides a potentially generalizable approach to accelerate the screening of complex materials whose structures can only be sampled from a distribution, e.g. amorphous polymers, surface defects, etc., because only one, instead of several, simulation needs to be performed for each material by adopting our approach.

The systematic error reduction demonstrated in this work is closely related to the transfer learning studies that aim to combine data from different sources [20, 22, 51, 52]. Our unique contribution in this work is to demonstrate the value of short, unconverged MD simulations in the context of material screening. We find that the systematic error between the 5 ns and 50 ns simulated transport properties can be corrected with a small amount of 50 ns simulations, which can potentially be generalized to other types of materials, properties, and simulation methods. In summary, we hope that the random and systematic error reductions observed in this work could highlight the value of imperfect, cheaper simulations for material screening that might previously be overlooked. A broader class of complex materials could be screened with a similar approach if a cheap, noisy, and biased simulation method can be identified.

METHODS

Graph representation for polymers. The polymers are represented by graphs based on their monomer structure. The node embeddings \mathbf{v}_i and edge embeddings \mathbf{u}_{ij} are initialized using atom and bond features described in Table S4 and S5. An additional edge is added to connect two ends of the monomer, allowing the end atoms to know the local chemical environments. We find that this representation has a better performance than using dummy atoms to denote the monomer ends.

Network architecture. We employ a graph convolution function developed in ref. [35] to learn the node embeddings in the graph. For each node i , we first concatenate the center

node, neighbor, and edge embeddings from last iteration $\mathbf{z}_{(i,j)}^{(t-1)} = \mathbf{v}_i^{(t-1)} \parallel \mathbf{v}_j^{(t-1)} \parallel \mathbf{u}_{(i,j)}$, then perform graph convolution,

$$\mathbf{v}_i^{(t)} = \mathbf{v}_i^{(t-1)} + \sum_{j \in \text{Neigh}(i)} \sigma(\mathbf{z}_{(i,j)}^{(t-1)} \mathbf{W}_f^{(t-1)} + \mathbf{b}_f^{(t-1)}) \cdot g(\mathbf{z}_{(i,j)}^{(t-1)} \mathbf{W}_s^{(t-1)} + \mathbf{b}_s^{(t-1)}), \quad (5)$$

where $\mathbf{W}_f^{(t-1)}$, $\mathbf{W}_s^{(t-1)}$, $\mathbf{b}_f^{(t-1)}$, $\mathbf{b}_s^{(t-1)}$ are weights, σ and g are sigmoid and softplus functions, respectively. After learning the node embeddings, we use a global soft attention pooling developed in ref. [53] to learn a graph embedding,

$$\mathbf{v}_G = \sum_i \text{softmax}(h_{\text{gate}}(\mathbf{v}_i)) \cdot h(\mathbf{v}_i), \quad (6)$$

where $h_{\text{gate}} : \mathbb{R}^F \rightarrow \mathbb{R}$ and $h : \mathbb{R}^F \rightarrow \mathbb{R}^F$ are two fully connected neural networks. The graph embedding \mathbf{v}_G is then used in Eq. 2 and Eq. 3 to predict polymer properties.

Molecular dynamics simulations. The molecular dynamics simulations are performed with the large atomic molecular massively parallel simulator (LAMMPS) [54]. The atomic interactions are described by the polymer consistent force-field (PCFF+) [55, 56], which has been previously used for polymer electrolyte systems [10, 11, 57]. The charge distribution of TFSI⁻ is adjusted following ref. [58], using a charge scaling factor of 0.7, to better describe the ion-ion interactions. All partial charges are reported in Table S6. There are 50 Li⁺ and TFSI⁻ in the simulation box. Each polymer chain has 150 atoms in the backbone. The number of polymer chains is determined by fixing the molality of LiTFSI at 1.5 mol/kg. The initial configurations are generated using a Monte Carlo algorithm, implemented in the MedeA simulation environment [59]. The 5 ns long equilibration procedure is based on a scheme described in ref. [11]. Once equilibrated, the system is then run in the canonical ensemble (nVT) at a temperature of 353 K, using a rRESPA multi-timescale integrator [60] with an outer timestep of 2 fs for non-bonded interactions, and an inner timestep of 0.5 fs. The high throughput workflow is implemented using the FireWorks workflow system [61].

Calculation of transport properties. The diffusivities of lithium and TFSI ions are calculated using the mean squared displacement (MSD) of the corresponding particles,

$$D = \frac{\langle [\mathbf{x}_i(t) - \mathbf{x}_i(0)]^2 \rangle}{6t}, \quad (7)$$

where \mathbf{x} is the position of the particle, t is the simulation time, and $\langle \cdot \rangle$ denotes an ensemble average over the particles. The diffusivity of the polymer is calculated by averaging the

diffusivities of O, N, and S atoms in the polymer chains. The conductivity of the entire polymer electrolyte is calculated using the cluster Nernst-Einstein approach developed in ref. [57]. This method takes into account ion-ion interactions in the form of aggregation of ion clusters,

$$\sigma = \frac{e^2}{Vk_B T} \sum_{i=0}^{N_+} \sum_{j=0}^{N_-} z_{ij}^2 \alpha_{ij} D_{ij}, \quad (8)$$

where α_{ij} is population of the ion clusters containing i cations and j anions, z_{ij} , D_{ij} are the charge and diffusivity of the cluster, N_+ and N_- are the maximum number of cations and anions in the clusters, e is the elementary charge, k_B is the Boltzmann constant, and V and T are the volume and the temperature of the system. We use the cNE₀ approximation that assumes D_{ij} is equal to the average diffusivity of lithium ion if the cluster is positively charged, and TFSI ion if the cluster is negatively charged. [57].

Data availability. The toy LogP dataset, the 5 ns and 50 ns MD datasets are available at URL. The experimentally measured conductivity from literature is available at supplementary Table S3. The MD trajectories will be made available in a future publication.

Code availability. The multi-task graph neural network is implemented with PyTorch [62] and PyTorch Geometric [63]. The code is available at URL.

-
- [1] Daniel T Hallinan Jr and Nitash P Balsara, “Polymer electrolytes,” *Annual review of materials research* **43**, 503–525 (2013).
 - [2] RC Agrawal and GP Pandey, “Solid polymer electrolytes: materials designing and all-solid-state battery applications: an overview,” *Journal of Physics D: Applied Physics* **41**, 223001 (2008).
 - [3] Koh Sing Ngai, S Ramesh, K Ramesh, and Joon Ching Juan, “A review of polymer electrolytes: fundamental, approaches and applications,” *Ionics* **22**, 1259–1279 (2016).
 - [4] Danielle M Pesko, Yukyung Jung, Alexandra L Hasan, Michael A Webb, Geoffrey W Coates, Thomas F Miller III, and Nitash P Balsara, “Effect of monomer structure on ionic conductivity in a systematic set of polyester electrolytes,” *Solid State Ionics* **289**, 118–124 (2016).
 - [5] Yoichi Tominaga, Tomoki Shimomura, and Mizuki Nakamura, “Alternating copolymers of carbon dioxide with glycidyl ethers for novel ion-conductive polymer electrolytes,” *Polymer*

- 51**, 4295–4298 (2010).
- [6] Leire Meabe, Nerea Lago, Laurent Rubatat, Chunmei Li, Alejandro J Müller, Haritz Sardon, Michel Armand, and David Mecerreyes, “Polycondensation as a versatile synthetic route to aliphatic polycarbonates for solid polymer electrolytes,” *Electrochimica Acta* **237**, 259–266 (2017).
- [7] Kan Hatakeyama-Sato, Toshiki Tezuka, Momoka Umeki, and Kenichi Oyaizu, “Ai-assisted exploration of superionic glass-type li⁺ conductors with aromatic structures,” *Journal of the American Chemical Society* **142**, 3301–3305 (2020).
- [8] Michael A Webb, Yukyung Jung, Danielle M Pesko, Brett M Savoie, Umi Yamamoto, Geoffrey W Coates, Nitash P Balsara, Zhen-Gang Wang, and Thomas F Miller III, “Systematic computational and experimental investigation of lithium-ion transport mechanisms in polyester-based polymer electrolytes,” *ACS central science* **1**, 198–205 (2015).
- [9] Brett M Savoie, Michael A Webb, and Thomas F Miller III, “Enhancing cation diffusion and suppressing anion diffusion via lewis-acidic polymer electrolytes,” *The journal of physical chemistry letters* **8**, 641–646 (2017).
- [10] Arthur France-Lanord, Yanming Wang, Tian Xie, Jeremiah A Johnson, Yang Shao-Horn, and Jeffrey C Grossman, “Effect of chemical variations in the structure of poly (ethylene oxide)-based polymers on lithium transport in concentrated electrolytes,” *Chemistry of Materials* **32**, 121–126 (2019).
- [11] Nicola Molinari, Jonathan P Mailoa, and Boris Kozinsky, “Effect of salt concentration on ion clustering and transport in polymer solid electrolytes: a molecular dynamics study of peo–litfsi,” *Chemistry of Materials* **30**, 6298–6306 (2018).
- [12] Keith T Butler, Daniel W Davies, Hugh Cartwright, Olexandr Isayev, and Aron Walsh, “Machine learning for molecular and materials science,” *Nature* **559**, 547–555 (2018).
- [13] Jonathan Schmidt, Mário RG Marques, Silvana Botti, and Miguel AL Marques, “Recent advances and applications of machine learning in solid-state materials science,” *npj Computational Materials* **5**, 1–36 (2019).
- [14] Rafael Gómez-Bombarelli, Jorge Aguilera-Iparraguirre, Timothy D Hirzel, David Duvenaud, Dougal Maclaurin, Martin A Blood-Forsythe, Hyun Sik Chae, Markus Einzinger, Dong-Gwang Ha, Tony Wu, *et al.*, “Design of efficient molecular organic light-emitting diodes by a high-throughput virtual screening and experimental approach,” *Nature materials* **15**, 1120–1127

- (2016).
- [15] Weike Ye, Chi Chen, Zhenbin Wang, Iek-Heng Chu, and Shyue Ping Ong, “Deep neural networks for accurate predictions of crystal stability,” *Nature communications* **9**, 1–6 (2018).
 - [16] Zeeshan Ahmad, Tian Xie, Chinmay Maheshwari, Jeffrey C Grossman, and Venkatasubramanian Viswanathan, “Machine learning enabled computational screening of inorganic solid electrolytes for suppression of dendrite formation in lithium metal anodes,” *ACS central science* **4**, 996–1006 (2018).
 - [17] Maarten De Jong, Wei Chen, Randy Notestine, Kristin Persson, Gerbrand Ceder, Anubhav Jain, Mark Asta, and Anthony Gamst, “A statistical learning framework for materials science: application to elastic moduli of k-nary inorganic polycrystalline compounds,” *Scientific reports* **6**, 34256 (2016).
 - [18] David Rolnick, Andreas Veit, Serge Belongie, and Nir Shavit, “Deep learning is robust to massive label noise,” *arXiv preprint arXiv:1705.10694* (2017).
 - [19] Bo Du, Tang Xinyao, Zengmao Wang, Lefei Zhang, and Dacheng Tao, “Robust graph-based semisupervised learning for noisy labeled data via maximum correntropy criterion,” *IEEE transactions on cybernetics* **49**, 1440–1453 (2018).
 - [20] Hironao Yamada, Chang Liu, Stephen Wu, Yukinori Koyama, Shenghong Ju, Junichiro Shiomi, Junko Morikawa, and Ryo Yoshida, “Predicting materials properties with little data using shotgun transfer learning,” *ACS central science* **5**, 1717–1730 (2019).
 - [21] Dipendra Jha, Kamal Choudhary, Francesca Tavazza, Wei-keng Liao, Alok Choudhary, Carolyn Campbell, and Ankit Agrawal, “Enhancing materials property prediction by leveraging computational and experimental data using deep transfer learning,” *Nature communications* **10**, 1–12 (2019).
 - [22] Justin S Smith, Benjamin T Nebgen, Roman Zubatyuk, Nicholas Lubbers, Christian Devereux, Kipton Barros, Sergei Tretiak, Olexandr Isayev, and Adrian E Roitberg, “Approaching coupled cluster accuracy with a general-purpose neural network potential through transfer learning,” *Nature communications* **10**, 1–8 (2019).
 - [23] Stephen Wu, Yukiko Kondo, Masa-aki Kakimoto, Bin Yang, Hironao Yamada, Isao Kuwajima, Guillaume Lambard, Kenta Hongo, Yibin Xu, Junichiro Shiomi, *et al.*, “Machine-learning-assisted discovery of polymers with high thermal conductivity using a molecular design algorithm,” *Npj Computational Materials* **5**, 1–11 (2019).

- [24] John J Irwin and Brian K Shoichet, “Zinc- a free database of commercially available compounds for virtual screening,” *Journal of chemical information and modeling* **45**, 177–182 (2005).
- [25] Danielle M Pesko, Michael A Webb, Yukyung Jung, Qi Zheng, Thomas F Miller III, Geoffrey W Coates, and Nitash P Balsara, “Universal relationship between conductivity and solvation-site connectivity in ether-based polymer electrolytes,” *Macromolecules* **49**, 5244–5255 (2016).
- [26] Qi Zheng, Danielle M Pesko, Brett M Savoie, Ksenia Timachova, Alexandra L Hasan, Mackensie C Smith, Thomas F Miller III, Geoffrey W Coates, and Nitash P Balsara, “Optimizing ion transport in polyether-based electrolytes for lithium batteries,” *Macromolecules* **51**, 2847–2858 (2018).
- [27] Yoichi Tominaga, “Ion-conductive polymer electrolytes based on poly (ethylene carbonate) and its derivatives,” *Polymer Journal* **49**, 291–299 (2017).
- [28] Jonas Mindemark, Laura Imholt, José Montero, and Daniel Brandell, “Allyl ethers as combined plasticizing and crosslinkable side groups in polycarbonate-based polymer electrolytes for solid-state li batteries,” *Journal of Polymer Science Part A: Polymer Chemistry* **54**, 2128–2135 (2016).
- [29] Carla Polo Fonseca, Derval S Rosa, Flávia Gaboardi, and Silmara Neves, “Development of a biodegradable polymer electrolyte for rechargeable batteries,” *Journal of power sources* **155**, 381–384 (2006).
- [30] Takahito Itoh, Kaito Nakamura, Takahiro Uno, and Masataka Kubo, “Thermal and electrochemical properties of poly (2, 2-dimethoxypropylene carbonate)-based solid polymer electrolyte for polymer battery,” *Solid State Ionics* **317**, 69–75 (2018).
- [31] İlknur Bayrak Pehlivan, Roser Marsal, Peter Georén, Claes G Granqvist, and Gunnar A Niklasson, “Ionic relaxation in polyethyleneimine-lithium bis (trifluoromethylsulfonyl) imide polymer electrolytes,” *Journal of Applied Physics* **108**, 074102 (2010).
- [32] Weisheng He, Zili Cui, Xiaochen Liu, Yanyan Cui, Jingchao Chai, Xinhong Zhou, Zhihong Liu, and Guanglei Cui, “Carbonate-linked poly (ethylene oxide) polymer electrolytes towards high performance solid state lithium batteries,” *Electrochimica Acta* **225**, 151–159 (2017).
- [33] MARCA M Doeff, L Edman, SE Sloop, J Kerr, and LC De Jonghe, “Transport properties of binary salt polymer electrolytes,” *Journal of Power Sources* **89**, 227–231 (2000).

- [34] Maria Manuela Silva, Paula Barbosa, Alan Evans, and Michael John Smith, “Novel solid polymer electrolytes based on poly (trimethylene carbonate) and lithium hexafluoroantimonate,” *Solid state sciences* **8**, 1318–1321 (2006).
- [35] Tian Xie and Jeffrey C Grossman, “Crystal graph convolutional neural networks for an accurate and interpretable prediction of material properties,” *Physical review letters* **120**, 145301 (2018).
- [36] Minggang Zeng, Jatin Nitin Kumar, Zeng Zeng, Ramasamy Savitha, Vijay Ramaseshan Chandrasekhar, and Kedar Hippalgaonkar, “Graph convolutional neural networks for polymers property prediction,” arXiv preprint arXiv:1811.06231 (2018).
- [37] Peter C St. John, Caleb Phillips, Travis W Kemper, A Nolan Wilson, Yanfei Guan, Michael F Crowley, Mark R Nimlos, and Ross E Larsen, “Message-passing neural networks for high-throughput polymer screening,” *The Journal of chemical physics* **150**, 234111 (2019).
- [38] Zhenqin Wu, Bharath Ramsundar, Evan N Feinberg, Joseph Gomes, Caleb Geniesse, Aneesh S Pappu, Karl Leswing, and Vijay Pande, “Moleculenet: a benchmark for molecular machine learning,” *Chemical science* **9**, 513–530 (2018).
- [39] Scott A Wildman and Gordon M Crippen, “Prediction of physicochemical parameters by atomic contributions,” *Journal of chemical information and computer sciences* **39**, 868–873 (1999).
- [40] RDKit, online, “RDKit: Open-source cheminformatics,” <http://www.rdkit.org>, [Online; accessed 11-April-2013].
- [41] Darko Butina, “Unsupervised data base clustering based on daylight’s fingerprint and tanimoto similarity: A fast and automated way to cluster small and large data sets,” *Journal of Chemical Information and Computer Sciences* **39**, 747–750 (1999).
- [42] DE Fenton, “Complexes of alkali metal ions with poly (ethylene oxide),” *polymer* **14**, 589 (1973).
- [43] Yoichi Tominaga and Kenta Yamazaki, “Fast li-ion conduction in poly (ethylene carbonate)-based electrolytes and composites filled with tio 2 nanoparticles,” *Chemical communications* **50**, 4448–4450 (2014).
- [44] Yoichi Tominaga, Kenta Yamazaki, and Vannasa Nanthana, “Effect of anions on lithium ion conduction in poly (ethylene carbonate)-based polymer electrolytes,” *Journal of the Electrochemical Society* **162**, A3133 (2015).

- [45] Alexander L Agapov and Alexei P Sokolov, “Decoupling ionic conductivity from structural relaxation: a way to solid polymer electrolytes?” *Macromolecules* **44**, 4410–4414 (2011).
- [46] Devansh Arpit, Stanisław Jastrzebski, Nicolas Ballas, David Krueger, Emmanuel Bengio, Maxinder S Kanwal, Tegan Maharaj, Asja Fischer, Aaron Courville, Yoshua Bengio, *et al.*, “A closer look at memorization in deep networks,” arXiv preprint arXiv:1706.05394 (2017).
- [47] Bo Han, Quanming Yao, Xingrui Yu, Gang Niu, Miao Xu, Weihua Hu, Ivor Tsang, and Masashi Sugiyama, “Co-teaching: Robust training of deep neural networks with extremely noisy labels,” in *Advances in neural information processing systems* (2018) pp. 8527–8537.
- [48] Nikolay Borodinov, Sabine Neumayer, Sergei V Kalinin, Olga S Ovchinnikova, Rama K Vasudevan, and Stephen Jesse, “Deep neural networks for understanding noisy data applied to physical property extraction in scanning probe microscopy,” *npj Computational Materials* **5**, 1–8 (2019).
- [49] Seoin Back, Kevin Tran, and Zachary W Ulissi, “Toward a design of active oxygen evolution catalysts: insights from automated density functional theory calculations and machine learning,” *ACS Catalysis* **9**, 7651–7659 (2019).
- [50] Seoin Back, Junwoong Yoon, Nianhan Tian, Wen Zhong, Kevin Tran, and Zachary W Ulissi, “Convolutional neural network of atomic surface structures to predict binding energies for high-throughput screening of catalysts,” *The journal of physical chemistry letters* **10**, 4401–4408 (2019).
- [51] Ekin D Cubuk, Austin D Sendek, and Evan J Reed, “Screening billions of candidates for solid lithium-ion conductors: A transfer learning approach for small data,” *The Journal of chemical physics* **150**, 214701 (2019).
- [52] Taishan Zhu, Sheng Gong, Tian Xie, Prashun Gorai, and Jeffrey C Grossman, “Charting lattice thermal conductivity of inorganic crystals,” arXiv preprint arXiv:2006.11712 (2020).
- [53] Yujia Li, Daniel Tarlow, Marc Brockschmidt, and Richard Zemel, “Gated graph sequence neural networks,” arXiv preprint arXiv:1511.05493 (2015).
- [54] Steve Plimpton, “Fast parallel algorithms for short-range molecular dynamics,” *Journal of computational physics* **117**, 1–19 (1995).
- [55] Huai Sun, “Force field for computation of conformational energies, structures, and vibrational frequencies of aromatic polyesters,” *Journal of Computational Chemistry* **15**, 752–768 (1994).
- [56] David Rigby, Huai Sun, and BE Eichinger, “Computer simulations of poly (ethylene oxide):

- force field, pvt diagram and cyclization behaviour,” *Polymer International* **44**, 311–330 (1997).
- [57] Arthur France-Lanord and Jeffrey C Grossman, “Correlations from ion pairing and the nernst-einstein equation,” *Physical review letters* **122**, 136001 (2019).
- [58] Marcelo J Monteiro, Fernanda FC Bazito, Leonardo JA Siqueira, Mauro CC Ribeiro, and Roberto M Torresi, “Transport coefficients, raman spectroscopy, and computer simulation of lithium salt solutions in an ionic liquid,” *The Journal of Physical Chemistry B* **112**, 2102–2109 (2008).
- [59] “MedeA-3.0, Materials Design, Inc, San Diego, CA USA,” (2020).
- [60] MBBJM Tuckerman, Bruce J Berne, and Glenn J Martyna, “Reversible multiple time scale molecular dynamics,” *The Journal of chemical physics* **97**, 1990–2001 (1992).
- [61] Anubhav Jain, Shyue Ping Ong, Wei Chen, Bharat Medasani, Xiaohui Qu, Michael Kocher, Miriam Brafman, Guido Petretto, Gian-Marco Rignanese, Geoffroy Hautier, *et al.*, “Fireworks: a dynamic workflow system designed for high-throughput applications,” *Concurrency and Computation: Practice and Experience* **27**, 5037–5059 (2015).
- [62] Adam Paszke, Sam Gross, Francisco Massa, Adam Lerer, James Bradbury, Gregory Chanan, Trevor Killeen, Zeming Lin, Natalia Gimelshein, Luca Antiga, *et al.*, “Pytorch: An imperative style, high-performance deep learning library,” in *Advances in neural information processing systems* (2019) pp. 8026–8037.
- [63] Matthias Fey and Jan E. Lenssen, “Fast graph representation learning with PyTorch Geometric,” in *ICLR Workshop on Representation Learning on Graphs and Manifolds* (2019).

ADDITIONAL INFORMATION

Acknowledgements This work was supported by Toyota Research Institute. Computational support was provided by the National Energy Research Scientific Computing Center, a DOE Office of Science User Facility supported by the Office of Science of the U.S. Department of Energy under Contract No. DE-AC02-05CH11231, and the Extreme Science and Engineering Discovery Environment, supported by National Science Foundation grant number ACI-1053575. J.L. acknowledges support by an appointment to the Intelligence Community Postdoctoral Research Fellowship Program at the Massachusetts Institute of Technology, administered by Oak Ridge Institute for Science and Education through an in-

teragency agreement between the U.S. Department of Energy and the Office of the Director of National Intelligence.

Author contributions. T.X. developed the software, performed the simulation and analysis. A.F.-L., T.X., and Y.W. designed the molecular dynamics simulation and analysis approaches. T.X., M.A.S., M.H. designed the polymer candidate space. J.L. gathered the data from literature. T.X. and J.C.G. conceived the idea and approach. All authors contributed to the interpretation of the results and the writing of the paper.

Competing interests. The authors declare no competing interests.

Materials & Correspondence. Correspondence and requests for materials should be addressed to T.X. (txie@mit.edu) and J.C.G. (jcg@mit.edu).

**Supplementary Information: Accelerating the screening of
amorphous polymer electrolytes by learning to reduce random
and systematic errors in molecular dynamics simulations**

Xie et al.

SUPPLEMENTARY NOTES

Supplementary Note 1: estimate true prediction error from noisy data.

We assume there exists a deterministic function f that maps from the polymer structure \mathcal{G} to its true target property. However, due to the random errors associated with the initial configuration in MD simulations, the simulated target property t has a small random error ϵ ,

$$t = f(\mathcal{G}) + \epsilon, \tag{S1}$$

where ϵ follows a normal distribution with zero bias $\mathcal{N}(0, \eta)$. Here, we assume that ϵ is not a function of \mathcal{G} , i.e. different polymers have the same random error independent of their structure. This assumption is approximately correct based on the differences in conductivity of the same polymer between two independent MD simulations in the log scale (Fig. S2).

To estimate the true prediction error of our model, we write our graph neural network model as a deterministic function g that predicts polymer property based on their structure \mathcal{G} ,

$$y = g(\mathcal{G}). \tag{S2}$$

Note that we use different labels for the predicted property y and the MD simulated property t .

Under these assumptions, the mean squared error between ML predictions and MD simulated properties, i.e. apparent prediction error, is,

$$\text{MSE}(y, t) = \mathbb{E}_{\mathcal{G}}[(y - t)^2] = \mathbb{E}_{\mathcal{G}}[(y - f(\mathcal{G}) - \epsilon)^2] = \mathbb{E}_{\mathcal{G}}[(y - f(\mathcal{G}))^2] + \mathbb{E}_{\mathcal{G}}[\epsilon^2]. \tag{S3}$$

Note that in the last step we use the fact that $\mathbb{E}_{\mathcal{G}}[\epsilon] = 0$.

The mean squared error between two independent MD simulations for the same polymer is,

$$\text{MSE}(t_1, t_2) = \mathbb{E}_{\mathcal{G}}[(t_1 - t_2)^2] = \mathbb{E}_{\mathcal{G}}[(\epsilon_1 - \epsilon_2)^2] = 2\mathbb{E}_{\mathcal{G}}[\epsilon^2]. \tag{S4}$$

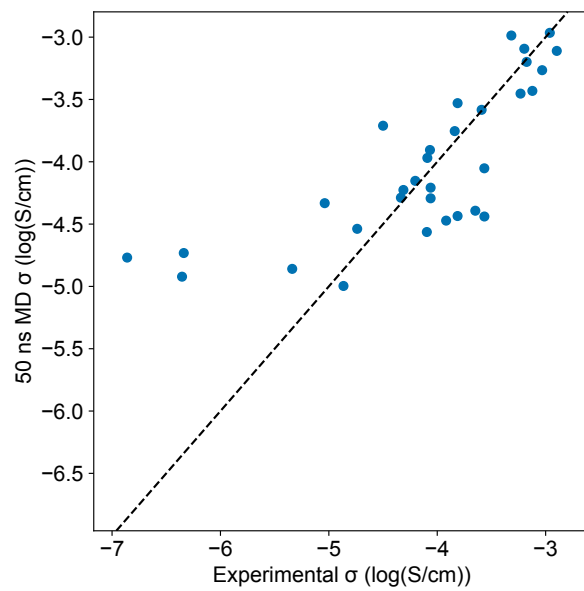
Therefore, the mean squared error between ML predictions and the true target property, i.e. true prediction error, is,

$$\text{MSE}(y, f(\mathcal{G})) = \mathbb{E}_{\mathcal{G}}[(y - f(\mathcal{G}))^2] = \text{MSE}(y, t) - \text{MSE}(t_1, t_2)/2. \tag{S5}$$

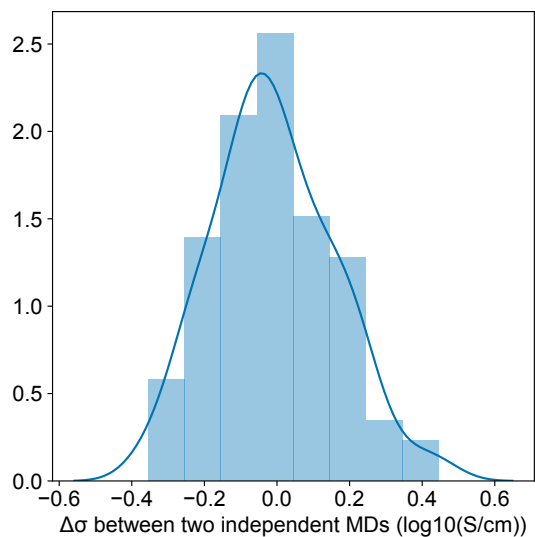
Based on our predictions on 86 testing data, $\text{MSE}(y, t) = 0.0209$ and $\text{MSE}(t_1, t_2) = 0.0274$. Therefore, the true prediction error $\text{MSE}(y, f(\mathcal{G})) = 0.0072$. In comparison, the

random error $\eta^2 \approx \mathbb{E}_{\mathcal{G}}[\epsilon^2] = 0.0137$. Remember that random errors can be reduced by running multiple MD simulations on the same polymers and computing the mean of target properties. Since $\eta_n = \eta/\sqrt{n}$, we estimate our ML prediction accuracy is approximately the accuracy of running $1.9 \approx 2$ MD simulations for each polymer.

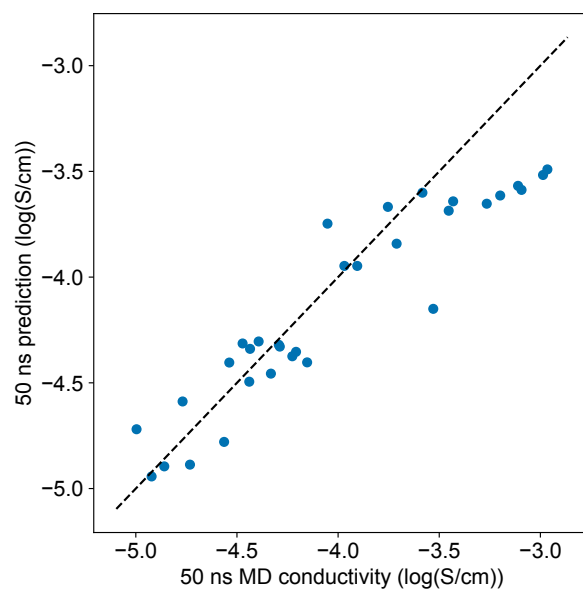
SUPPLEMENTARY FIGURES



Supplementary Figure S1. Comparison between 50 ns MD simulated conductivity and experimental conductivity reported in literature at the same salt concentration and temperature.



Supplementary Figure S2. Differences in conductivity of the same polymer between two independent 5 ns molecular dynamics simulations.



Supplementary Figure S3. Comparison between 50 ns MD and predicted conductivity for the polymers from literature.

SUPPLEMENTARY TABLES

Supplementary Table S1. Molecular structure, simulated conductivity, and predicted conductivity for the top polymers in the search space.

SMILES	50 ns MD σ	Predicted σ
<chem>CN(CCCO[Cu])CCOCCOC(=O)[Au]</chem>	-3.74	-3.95
<chem>O=C([Au])NCCOCCOCCOCCO[Cu]</chem>	-3.76	-3.73
<chem>O=C([Au])OCCOCCCCOCCO[Cu]</chem>	-3.85	-3.90
<chem>O=C([Au])OCCCSCCOCCO[Cu]</chem>	-3.97	-3.95
<chem>O=C([Au])OCCCOCCCOCCO[Cu]</chem>	-4.00	-3.94
<chem>C=CCN(CCO[Cu])CCOCCOC(=O)[Au]</chem>	-4.00	-3.95
<chem>O=C([Au])NCCOCCOCCOCCN[Cu]</chem>	-4.00	-3.82
<chem>O=C([Au])OCCNCCOCCO[Cu]</chem>	-4.02	-3.85
<chem>NOCCNCC(COC(=O)[Au])O[Cu]</chem>	-4.10	-3.93
<chem>CN(CCO[Cu])CCOCCOC(=O)[Au]</chem>	-4.19	-3.92

Supplementary Table S3. Molecular structure, experiment conductivity, and predicted conductivity for polymers from literature.

SMILES	50 ns MD σ	Predicted σ
<chem>[Cu]CCOCCOCCOCCOCCOCC[Au]</chem>	-2.90	-3.57
<chem>[Cu]OCC[Au]</chem>	-2.96	-3.49
<chem>[Cu]CCCCCOCCOCCOCCOCCOCCOCC[Au]</chem>	-3.03	-3.65
<chem>[Cu]CCCCOCCOCCOCCOCCOCC[Au]</chem>	-3.12	-3.64
<chem>[Cu]CCCCOCCOCCOCCOCCOCCOCC[Au]</chem>	-3.18	-3.61
<chem>[Cu]CCOCCOCCOCCOCCOCC[Au]</chem>	-3.20	-3.59
<chem>[Cu]CCCCCOCCOCCOCCOCCOCC[Au]</chem>	-3.23	-3.69
<chem>[Cu]OCOCCOCC[Au]</chem>	-3.32	-3.52
<chem>[Cu]OC(CCCCC[Au])=O</chem>	-3.57	-4.49
<chem>[Cu]OC(=O)OCCOCCOCC[Au]</chem>	-3.57	-3.75
<chem>[Cu]OC(=O)OCCOCCOCCOCCOCCOCCOCC[Au]</chem>	-3.59	-3.60
<chem>[Cu]OC(=O)OCCCCCCCCCCC[Au]</chem>	-3.65	-4.30
<chem>[Cu]CC(C)O[Au]</chem>	-3.81	-4.15
<chem>[Cu]OC(=O)OCCCCCCC[Au]</chem>	-3.81	-4.34
<chem>[Cu]OC(=O)OCCOCCOCCOCCOCC[Au]</chem>	-3.84	-3.67
<chem>[Cu]OC(=O)OCCCCCCCCCCC[Au]</chem>	-3.92	-4.31
<chem>[Cu]OC(=O)OCCCCCCC[Au]</chem>	-4.06	-4.35
<chem>[Cu]OC(=O)OCCCCCCCCCCC[Au]</chem>	-4.06	-4.32
<chem>[Cu]OC(=O)OCCOCC[Au]</chem>	-4.07	-3.95
<chem>[Cu]C(=O)CCCC(=O)OC(C)CO[Au]</chem>	-4.10	-4.78
<chem>[Cu]OC(=O)OCCCC[Au]</chem>	-4.20	-4.40
<chem>[Cu]OC(=O)OCCCCC[Au]</chem>	-4.31	-4.37
<chem>[Cu]OC(=O)OCCCCCCCCC[Au]</chem>	-4.34	-4.33
<chem>[Cu]NCC[Au]</chem>	-4.50	-3.84
<chem>[Cu]C(=O)COCC(=O)OC(C)CO[Au]</chem>	-4.74	-4.40
<chem>[Cu]OC(=O)OCC(CC)(COCC=C)C[Au]</chem>	-4.87	-4.72
<chem>[Cu]OC(=O)OCCC[Au]</chem>	-5.04	-4.46
<chem>[Cu]OC(=O)OC(C)C[Au]</chem>	-5.34	-4.90
<chem>[Cu]OC(=O)OC(CC)C[Au]</chem>	-6.34	-4.89
<chem>[Cu]OC(=O)OC(CCC)C[Au]</chem>	-6.35	-4.94
<chem>[Cu]OC(=O)OCC(OC)(OC)C[Au]</chem>	-6.86	-4.59

Supplementary Table S4. Atom features.

Feature	Description
Atom type	Atomic number of elements (one-hot)
Degree	Atom degree (one-hot)
Formal charge	Formal charge of atoms (one-hot)
Number of hydrogen	Number of connected hydrogen atoms (one-hot)
Hybridization	Hybridization type of the atomic orbitals (one-hot)
Aromatic	Whether the atom belongs to an aromatic ring (binary)
Ring	Whether the atom belongs to a ring (binary)

Supplementary Table S5. Bond features.

Feature	Description
Bond type	Type of the bond, e.g. single, double, aromatic (one-hot)
Stereochemistry	Stereochemistry of the bond (one-hot)
Conjugated	Whether the bond is conjugated (binary)

Supplementary Table S6. Partial charges of the ions.

Species	Charge (e)
Li	+0.7000
S	+0.3395
C	+0.2100
F	-0.0826
O	-0.2513
N	-0.2982